Improving the mechanical properties of polycaprolactone using functionalized nanofibrillated bacterial cellulose with high dispersibility and long fiber length as a reinforcement material

Hamidah binti Hashim,[a] Nur Aisyah Adlin binti Emran,[a] Takuya Isono,[b] Satoshi Katsuhara,[a] Hiroko Ninoyu,[a] Tokuo Matsushima,[c] Takuya Yamamoto,[b] Redouane Borsali,[d] Toshifumi Satoh,[b] and Kenji Tajima[b] *

[a]Graduate School of Chemical Sciences and Engineering, Hokkaido University, Sapporo, 060-8628, Japan.

[b]Faculty of Engineering, Hokkaido University, Sapporo, 060-8628, Japan.

[c]Kusano Sakko Inc., Nishimachi 16, Kamiebetsu, Ebetsu, Hokkaido 067 0063, Japan.

[d]Univ Grenoble Alpes, CNRS, CERMAV, F-38000, Grenoble, France.

E-mail address:

bintihashim.hamidah.a7@elms.hokudai.ac.jp (H. H); **aisyahadlin96@gmail.com** (A.A); **isono.t@eng.hokudai.ac.jp** (T.I); **satoshi-k@eis.hokudai.ac.jp** (S.K); **hiroko-ninoyu@kureha.co.jp** (H.N); **t-matsushima@kusanosk.co.jp** (T.M); **yamamoto.t@eng.hokudai.ac.jp** (T.Y); **redouane.borsali@cermav.cnrs.fr** (R.B); **satoh@eng.hokudai.ac.jp** (T.S); **ktajima@eng.hokudai.ac.jp** (K.T)

***** Corresponding author Kenji Tajima

Tel.: +81(11)-706-6603; fax: +81(11)-706-6603

Email address: ktajima@eng.hokudai.ac.jp

Postal address: Faculty of Engineering, Hokkaido University, N13W8, Kita-ku, Sapporo 060-8628, Japan

Abstract

Nanofibrillated bacterial cellulose (NFBC) produced in the presence of hydroxypropylcellulose (HPC) (HP-NFBC) is amphiphilic and has a very long fiber length (>15 μm). In this study, polycaprolactone (PCL)-grafted HP-NFBC (HPNFBC-*g*-PCL) was prepared via ring-opening polymerization from the hydroxy groups on the HP-NFBC surface as initiation sites. The mechanical properties of the nanocomposites containing PCL homopolymer and HPNFBC-*g*-PCL were investigated. The nanocomposite with 13 wt.% cellulose was the stiffest film with the highest ultimate strength and Young's modulus of 57.3 and 661.3 MPa, respectively. HP-NFBCs grafted with PCL of different molecular weights (20, 15, and 9k) were also prepared to study the effect of the graft length on the mechanical properties of the nanocomposites. Grafting HP-NFBC with a higher molecular weight (20k) PCL led to an enhanced ultimate strength and Young's modulus. These results suggest that HP-NFBC can serve as an excellent reinforcement material.

Keywords:

A. Cellulose; A. Fibres; A. Polymer-matrix composites (PMCs); B. Mechanical properties

1. Introduction

Over the last few decades, there has been growing concern about the sustainability of petrochemical-based resources that cause a wide array of impacts on welfare, health, and ecosystems. Consequently, particular attention is being given to the production of biodegradable and biocompatible polymeric nanocomposite materials as sustainable resources for the future. Cellulose, the most abundant natural polymer on earth, has gained recognition as an excellent substitute for fossil-fuel-based materials because of its renewable and biodegradable properties. Cellulose is a major component of plant cell walls and is a naturally abundant linear homopolymer

consisting of $_{D}$-glucopyranose linked by β-1,4-glycosidic bonds [1,2]. Nanofibrillated bacterial cellulose (NFBC) can be produced from low molecular weight biomasses such as sugars, glycerol, and molasses via a bottom-up process using the cellulose-producing bacterium *Gluconacetobacter intermedius* (*G. intermedius*) NEDO-01 [3,4]. The NFBC produced by this process shows a relatively homogenous fiber width and very long fiber length (>15 μm) [5]. We reported the functionalization of NFBC with a dispersing agent, such as hydroxypropyl cellulose (HPC), which is an amphiphilic water-soluble cellulose derivative, to produce NFBC with HPC (HP-NFBC), which shows high dispersibility toward some polar organic solvents as well as water [6]. In addition, we successfully obtained poly(methyl methacrylate) (PMMA)/HP-NFBC nanocomposites having a higher tensile strength by a simple solvent mixing method [6]. Therefore, HP-NFBC has the potential to function as an efficient reinforcement material based on its excellent characteristics.

Poly(ε-caprolactone) (PCL), a commercially available biodegradable polymer, is a semi-crystalline, aliphatic polyester that has attracted much attention for decades because of its advantageous physical, chemical, and thermal properties, in addition to its biocompatibility, and biodegradability [7–9]. PCL can be synthesized via ring-opening polymerization (ROP) of ε-caprolactone (ε-CL). The limitations of PCL include its low modulus and tensile strength. The mechanical properties of PCL can be improved by reinforcement with cellulose nanofillers [10–12]. However, the incompatibility between the hydrophobic polymer matrices and hydrophilic cellulose restricts the use of nanocellulose fibers as a reinforcement (filler) material in biodegradable polymers [13–15] . Polymer grafting is an efficient approach to overcome this issue and control the properties of the involved interfaces [16–19]. The covalent introduction of polymers on the nanofiller surface is an efficient method of improving the interaction between the

cellulose nanofillers and polymer matrix by controlling the molecular weight of the grafted polymer. The "grafting-onto" method is a modular approach in which the polymers can be prepared prior to the grafting step, which ensures the efficient control of their molecular size and architecture [20–22]. However, graft densities may be limited due to steric hindrance between the incoming polymers. In addition, the reactions necessitate harsh conditions, *e.g*., high temperatures and long reaction times. In contrast, the "grafting-from" method achieves high grafting densities and the incorporation of high amounts of grafting polymers. Bellani *et al* [23] reported an improvement in the mechanical properties and an increase in the thermal stability and crystallization temperature of PCL chains grafted from cellulose nanocrystals. Lönnberg *et al* [24] reported that the mechanical properties of cellulose nanocomposite materials are significantly improved by increasing the polymer graft length.

A large number of PCL-grafted cellulose species have been studied involving both plant-based NFC and bacterial synthesized cellulose (BC). However, there have been no reports on nanocomposites where the effect of incorporating NFBC functionalized with HPC, consisting of a very long fiber length nanofiller, such as HP-NFBC, and exhibiting enhanced mechanical properties, has been studied. The high mechanical strength, aspect ratio (>500), dispersibility, and moldability of HP-NFBC [6] can noticeably improve the mechanical performance of nanocomposites. In the present work, the applicability of HP-NFBC as a reinforcement filler material was examined. The "grafting-from" method was used for synthesizing graft copolymers (HPNFBC-*g*-PCLs). Three graft copolymers (HPNFBC-*g*-PCLs) with PCLs of different molecular weights were synthesized using the "grafting-from" method. The influence of the graft length on the mechanical properties of the nanocomposites was evaluated. The synthesized HPNFBC-*g*-PCLs were characterized using Fourier-transform infra-red (FT-IR) spectroscopy, solid-state ^{13}C-

nuclear magnetic resonance (CP/MAS ^{13}C-NMR) spectroscopy, size-exclusion chromatography (SEC), differential scanning calorimetry (DSC), thermogravimetric analysis (TG), and atomic force microscopy (AFM). The HPNFBC-*g*-PCLs were mixed with PCL homopolymers in a solution state to produce nanocomposites containing 0, 1, 4, 7, and 13 wt.% of cellulose through solvent casting. The mechanical properties of the nanocomposites were evaluated using tensile tests and thermomechanical analysis (TMA).

2. Experimental

2.1. Materials

Dibenzyl ether (99 %) and *ε*-CL (>99 %) were purchased from Tokyo Chemical Industry Co., Ltd. (Tokyo, Japan). *ε*-CL was distilled and dibenzyl ether was used without further purification. Diphenyl phosphate (DPP, >99 %) and PCL (M_n, 87400 g mol^{-1}; $Đ$, 1.68) were purchased from Sigma-Aldrich Japan K.K. (Tokyo, Japan). Prior to grafting, the DPP was purified by azeotropic distillation with dry toluene several times and vacuum dried. Toluene (>99 %) and methanol (>99 %) were purchased from Kanto Chemical Co., Inc. (Tokyo, Japan) and used without further purification. HP-NFBC was supplied by Kusano Sakko Inc. (Ebetsu, Japan) (HPC content: 25 wt. %). HP-NFBC was washed three times with distilled water. Subsequently it was centrifuged several times (9000 rpm, 15 min, 25 °C) for further purification. After freezing at –80 °C for 2 h, the purified HP-NFBCs were lyophilized for 48 h. Prior to grafting, the HP-NFBCs were dried in an oven at 105 °C for 3 h to remove water molecules.

2.2. Preparation of PCL-grafted HP-NFBCs via a "grafting-from" method using ROP

PCL was grafted from HP-NFBC by ROP of the ε-CL monomer using DPP as the organocatalyst (**Scheme 1**) in accordance with a previously published report [25,26]. A typical procedure for the polymerization involved placing HP-NFBC (0.5 g) in a 200 mL round-bottom flask followed by the addition of the DPP catalyst, ε-CL monomer, and an appropriate amount of toluene were added into the flask in a dry box. The ROP was performed at 80 °C with continuous stirring. Dibenzyl ether was used as an internal standard to calculate the monomer conversion using ^{1}H NMR spectroscopy. After the reaction, the solution was diluted by adding excess amount of toluene to instantly terminate the polymerization and the reaction mixture was stirred at room temperature for 17 h. The mixture was then centrifuged three times at 10000 rpm for 60 min at 25 °C to remove the residual monomer, PCL homopolymer, and DPP. PCL-grafted HP-NFBC (HPNFBC-*g*-PCL) was obtained as a pellet. The pellet was dispersed in a small amount of toluene and precipitated using excess cold methanol. The precipitated HPNFBC-*g*-PCL was collected by filtration and dried overnight at room temperature *in vacuo*. The composites having HP-NFBC:ε-CL weight ratios of 1:20, 1:15, and 1:10 were denoted as HPNFBC-*g*-PCL-20, HPNFBC-*g*-PCL-15, and HPNFBC-*g*-PCL-10, respectively.

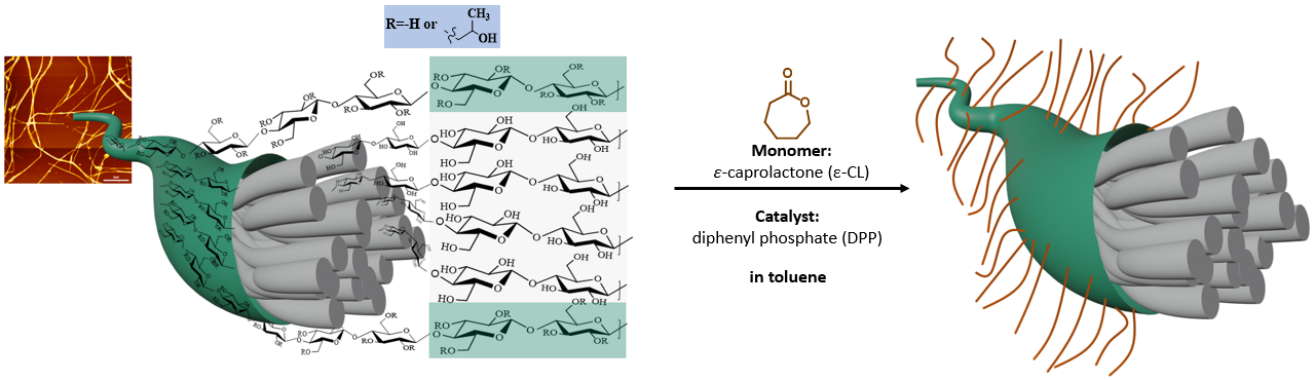

Scheme 1. Preparation of HPNFBC-*g*-PCL using a "grafting-from" method via ROP of ε-CL

2.3. Preparation of HPNFBC-g-PCL/PCL nanocomposites

HPNFBC-*g*-PCLs were dispersed in toluene (10 mL) at 80 °C for 1 d under stirring. After the HPNFBC-*g*-PCLs were fully dispersed, the desired amount of PCL was added and stirred at the same temperature for 2 h. The HPNFBC-*g*-PCL and PCL compositions were adjusted to prepare nanocomposites containing 0, 1, 4, 7, and 13 wt.% of HP-NFBC. The solutions were cast on Teflon Petri dishes, and the toluene was evaporated under a stream of air at 55 °C for 1 d prior to vacuum drying at 45 °C for 1 d to obtain solid films (thickness: 60–100 μm).

2.4. Structural analyses of HPNFBC-g-PCLs

FTIR spectroscopy. FT-IR spectra were recorded on a Perkin Elmer Frontier MIR/UATR instrument in attenuated total reflectance (ATR) mode at a running scan and resolution of 8 and 1 cm^{-1}, respectively. PCL and HPNFBC-*g*-PCLs spectra were normalized by a peak at 1723 cm^{-1} corresponding to C=O absorption based on PCL. No normalization was applied for HP-NFBC spectrum.

SEC measurements. The number-average molecular weight ($M_{n,SEC}$) and dispersity ($Đ$) were determined using SEC in THF (1.0 mL min^{-1}) which was performed on a Shodex KF-G guard column, Shodex KF-804L column, and Jasco CO-2065 Plus column oven. A Jasco DG-2080-53 was used as the degassing device. The SEC apparatus was calibrated with linear polystyrene standards [27].

^{1}H NMR spectroscopy. ^{1}H NMR spectra were recorded on a JEOL JNM-ECS400 (400 MHz) instrument at 25 °C using $CDCl_3$ as the solvent [internal standard: tetramethylsilane (TMS) (0.00 ppm); number of scans: 8].

Solid-state ^{13}C NMR spectroscopy Solid-state cross-polarization magic angle spinning ^{13}C NMR (^{13}C CP/MAS NMR) spectra were obtained using a DSX 300 spectrometer (Bruker, Germany) operating at 75.48 MHz. The samples were packed in a 4.0 mm rotor and spun at a frequency of 4 kHz at contact and recycle times of 1.0 ms and 4 s, respectively. The spectra were calibrated using the carbonyl carbon of glycine (chemical shift: 176.03 ppm) as a standard [28].

AFM studies. AFM images were obtained using a Hitachi AFM5000II instrument in tapping mode with a silicon cantilever (SI-DF3P2, SII Nanotechnology Inc.) having a resonant frequency and spring constant of 70 kHz and 2.1 N m^{-1}, respectively. The thin films for the AFM studies were prepared by dispersing the respective materials in toluene [0.05 (w/v) %], followed by depositing 5 μL of each dispersion on the surface of a mica substrate. The films were dried at 30 °C in a drying oven prior to observation.

2.5. Characterization of HPNFBC-g-PCL/PCL nanocomposites.

TG-DTG. The decomposition behavior of the samples was studied using a Hitachi STA200RV instrument. The samples (~5 mg) were heated from 25 to 600 °C at a heating rate of 10 °C min^{-1} under a nitrogen atmosphere.

DSC. The melting point was recorded using a Hitachi DSC 7000X instrument. The samples (~5 mg) were placed in aluminum pans and sealed hermetically. First, the samples were heated to 150 °C. They were subsequently cooled to -20 °C, and reheated to 150 °C. The cooling and heating rates were 20 and 10 °C min^{-1}, respectively. All the operations were performed under a nitrogen atmosphere. The crystallinity (χ_c) of each sample was calculated according to the following equation (eq. 1):

$$\chi_c = \Delta H_m / (w \times \Delta H^o_{100}), \quad (1)$$

where ΔH_m is the heat of fusion of the sample, w is the weight fraction of PCL, and ΔH_{100}^o is the heat of fusion of 100 % crystalline PCL, 136 J g^{-1} [29].

Tensile tests. Dumbbell-shaped specimens of the films with gauge lengths and widths of 12 and 2 mm, respectively, were prepared for tensile testing. The tensile tests were performed using an INSTRON 34SC-1 tensile tester with a cross-head speed of 10 mm min^{-1} under ambient condition. The measurement for each kind of film was repeated five times and reported as the mean value and standard deviation.

TMA. The coefficient of thermal expansion (CTE) was measured using a thermomechanical analyzer (Hitachi TMA7300) with a constant heating rate of 5 °C min^{-1} in the temperature range of 30 –100 °C.

3. Results and Discussions

3.1. Preparation of HPNFBC-g-PCLs via a "grafting-from" method using ROP.

Polymerization was performed using dry toluene as the solvent. PCLs with three different molecular weights were synthesized to obtain different graft lengths. The reaction compositions of the different polymerization systems are listed in **Table 1**. The polymerization reactions were terminated when the monomer conversions reached 90 % and above (**Figures S2–4**). Dibenzyl ether was used as an internal standard to determine the monomer conversions. The reactions were first conducted in bulk but it resulted in an extremely low cellulose percentage and uncontrollable amounts of grafted PCL due to the poor dispersion of the cellulose in the monomer. In contrast, the graft lengths, as well as the amounts of grafted PCL, were controllable when toluene was added

due to the efficient dispersion of HP-NFBC in organic solvents. The initiation reaction rates of the O-H groups of cellulose during the ROP of monomeric *ε*-CL were thus improved.

Table 1. Polymerization conditions and molecular parameters of HPNFBC-*g*-PCLs[a]

Sample	$w_{0,\,\varepsilon\text{-CL}}$/ $w_{0,\,\text{HP-NFBC}}$[b]	**Estimated M_n of grafted PCL[c]**	***Đ*[c]**	**PCL content[d] (mol%)**	**HP-NFBC content[d] (mol%)**
HPNFBC-*g*-PCL-10	10/1	8960	1.16	55.0	45.0
HPNFBC-*g*-PCL-15	15/1	13900	1.23	78.0	22.0
HPNFBC-*g*-PCL-20	20/1	20100	1.37	86.0	14.0

[a]Polymerization conditions: temperature, 80 °C; $[\varepsilon\text{-CL}]_0/[\text{DPP}]_0 = 1000/1$. [b]Mass ratio of *ε*-CL and HP-NFBC before polymerization. [c]Estimated by SEC analysis of the obtained free PCL homopolymers in THF with polystyrene standard; values corrected using correcting factor for PCL, 0.56. [d]Determined by CP/MAS ^{13}C NMR based on Equation S1 and S2.

3.2. Structural analyses of HPNFBC-g-PCLs.

Accurate determination of the molecular weights of the grafted PCLs often requires intricate techniques, such as the hydrolytic cleavage of interfacial ester bonds, which might be unfavorable for grafted PCLs. Therefore, SEC was performed to estimate the molecular weight of the grafted polymer by measuring the molecular weight of the un-grafted PCL (free homopolymer) [30,31] and the average molecular weight values were determined using a method previously reported [32]. The molecular weights of the PCL homopolymers formed during polymerization and the corresponding SEC traces are presented in **Table 1** and **Figure S5**, respectively. HPNFBC-*g*-PCL-20 with the highest monomer feed corresponded to the highest molecular weight of the PCL homopolymer and vice versa. This indicates that a higher amount of monomer feed leads to a higher molecular weight, which is in agreement with the results of a previous study [33]. The

amount of PCL grafted from the surface can be controlled by adjusting the ratio of the added monomer to the cellulose as the initiator [33]. The utility of the "grafting-from" method in controlling the polymer chain length is thus demonstrated.

The FT-IR spectra of HP-NFBC and HPNFBC-*g*-PCL are shown in **Figure 1**. HP-NFBC exhibits cellulose characteristic absorption bands at 3350 and 2890 cm^{-1} corresponding to the stretching vibrations of the hydroxyl (O-H) and alkyl groups (C-H), respectively [34]. After PCL grafting, all the samples displayed strong peaks corresponding to the carbonyl (C=O) stretching at 1723 cm^{-1}, which indicated the presence of PCL. C=O peak shown in PCL and all HPNFBC-*g*-PCLs were normalized to compare the difference in height of absorbance unit peak (y-axis) between C=O and O–H absorbance peak originated from PCL and HP-NFBC, respectively in each sample. The height of absorbance peak for C=O were normalized and kept as control peak to easily compare the changes in O–H absorbance peak changes. The peak's height differences were 7.70, 5.17 and 3.48 for HPNFBC-*g*-PCL-20, HPNFBC-*g*-PCL-15 and HPNFBC-*g*-PCL-10, respectively. The value showed increasing pattern as the grafted molecular weight of the PCL were increased which indicates the decreasing intensity O=H absorption. The intensity of the O-H absorption band decreased as the amount of *ε*-CL was increased, indicating that the grafting densities and amounts of grafted polymers could be controlled by varying the monomer feed. This is in agreement with the CP/MAS ^{13}C NMR results, discussed later. The ratio of PCL and HP-NFBC contents in each HPNFBC-*g*-PCL species were further investigated using CP/MAS ^{13}C NMR analysis (**Figure 2**). The PCL: HP-NFBC molar ratio (**Table 1**) in each HPNFBC-*g*-PCL sample was determined by comparing the C_1 peak of cellulose to the $C_{b\text{-}e}$ peak of PCL. For the calculations, the integral value of the C_1 peak of cellulose was set to 1 and the integral values were multiplied with the coefficients derived from the extrapolation of the CP time-relative magnetization graph obtained through NMR

relaxation time measurements (**Figures S6, S7**, and **Table S1**) [35]. The intensity of the peaks corresponding to PCL decreased gradually upon decreasing the monomer feed, which indicated that the amount of grafted PCL was successfully controlled by controlling the monomer feed to cellulose ratio.

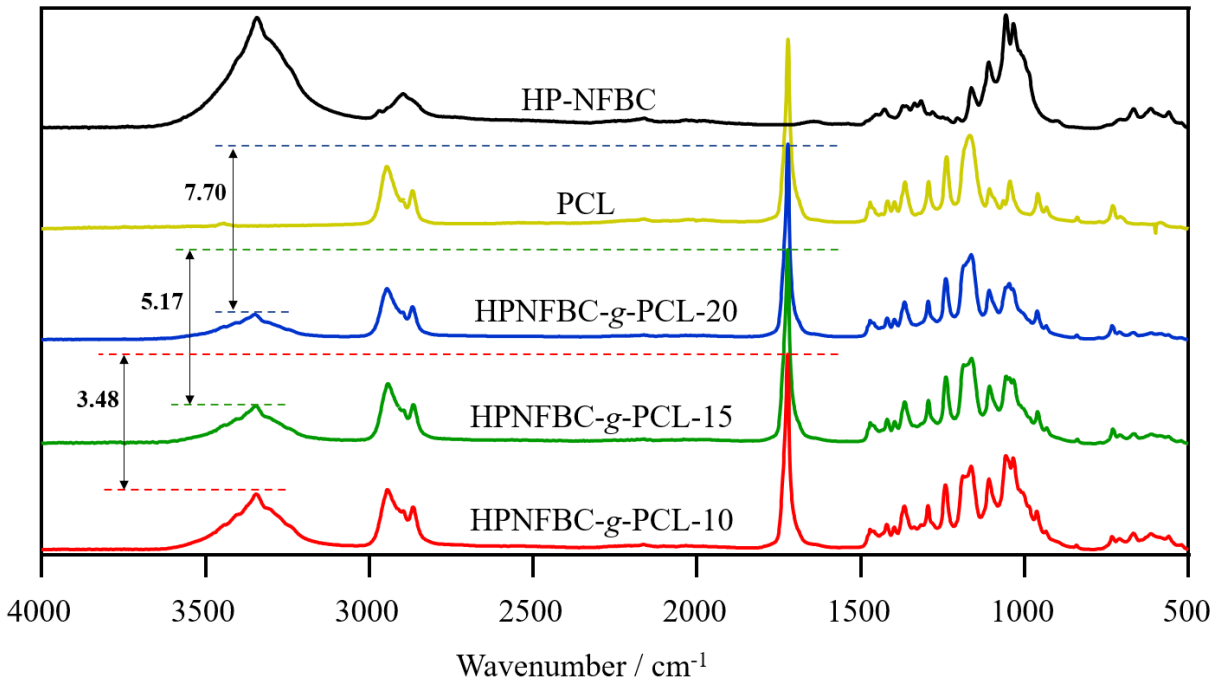

Figure 1. FT-IR (ATR) spectra of HP-NFBC, HPNFBC-*g*-PCLs, and PCL.

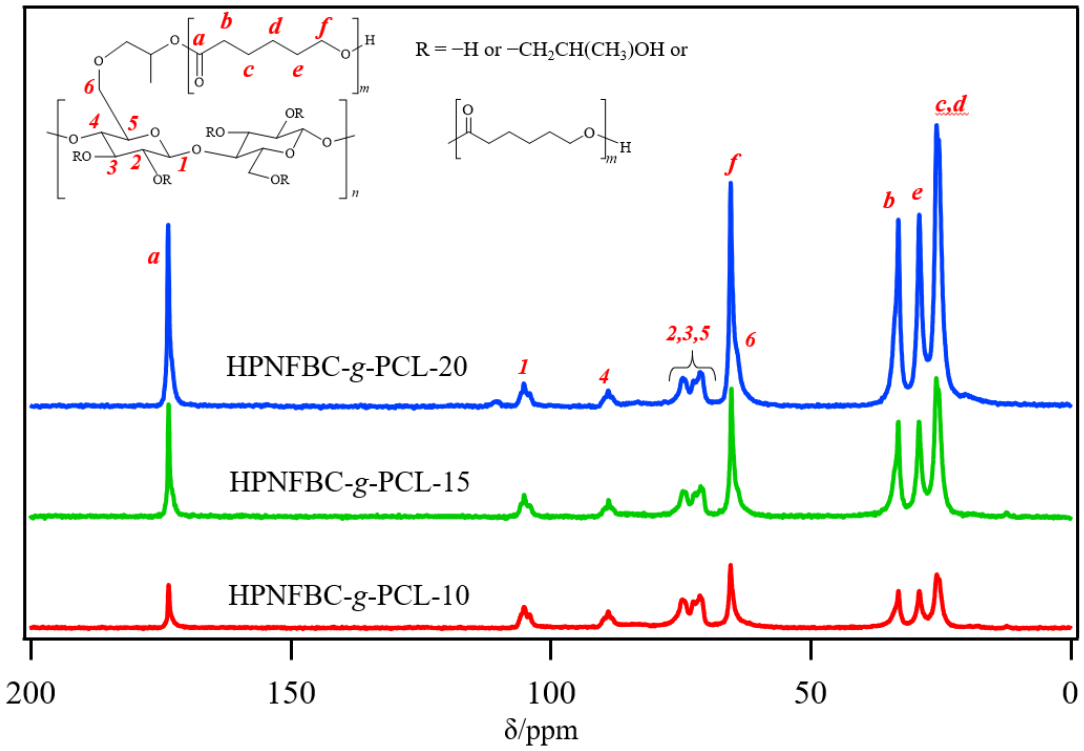

Figure 2. CP/MAS ^{13}C NMR spectra of HPNFBC-*g*-PCLs.

Upon AFM analyses of the three types of grafted PCL, unlike that of HPNFBC-*g*-PCL-20, the fiber image corresponding to the shorter PCL chain exhibited a poor resolution [**Figures S8 (a-d)**]. The morphologies of HP-NFBC and HPNFBC-*g*-PCL-20 were compared to determine the differences between the grafted and un-grafted morphologies [**Figures 3 (a-d)**]. The HP-NFBC fiber is thin and can be clearly seen in both the height and phase images, whereas in HPNFBC-*g*-PCL-20, the edges of the fiber are considerably blurry. In addition, the average fiber width of HPNFBC-*g*-PCL-20 was 2–3 times larger than that of the un-grafted HP-NFBC, indicating the presence of grafted PCL in HPNFBC-*g*-PCL-20. No micrometer-scale agglomeration was observed, suggesting improved hydrophobic characteristics. However, some agglomeration was observed for the dispersion of HPNFBC-*g*-PCL-10, which had a high HP-NFBC content of 45 % (**Figure S9**), which also contributed to the indistinct images. This phenomenon was reported

previously by Ansari & Berglund *et al* [36]. It is plausible that the minute fibrous projections along the principal fibers observed in HPNFBC-*g*-PCL resulted from the efficient crystallization of the densely packed PCL, which is discussed further in connection with the DSC analysis results.

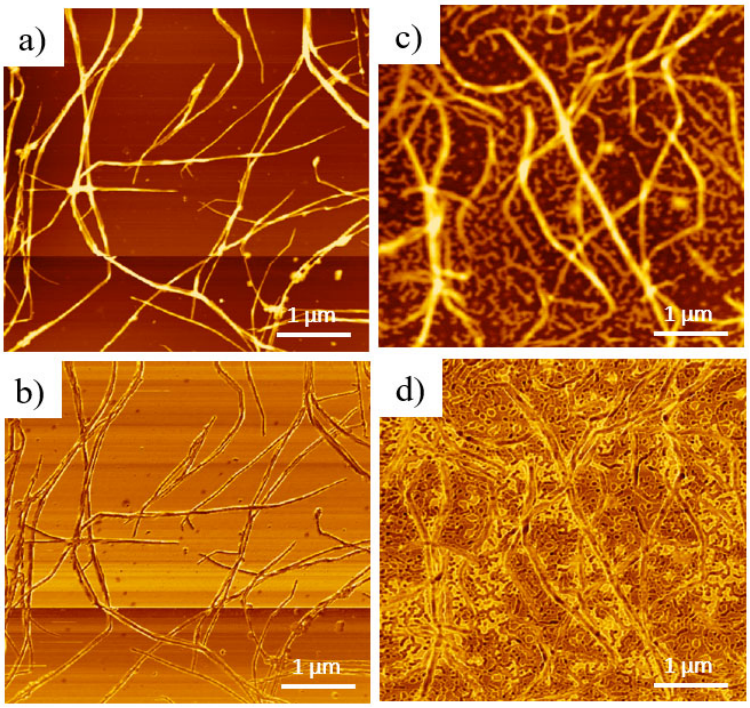

Figure 3. AFM images of HP-NFBC (a, height; b, phase) and HPNFBC-*g*-PCL-20 (c, height; d, phase).

3.3. Thermal properties of HPNFBC-g-PCLs.

The grafting of PCL onto HP-NFBC caused a significant change in thermal stability, as assessed by TG-DTG analyses. **Figures S10 (a)** and **(b)** show the TG and DTG curves of all the samples, and the results are summarized in **Table 2**. All the samples (HP-NFBC, PCL, and HPNFBC-*g*-PCLs) showed a single weight loss step, in which PCL had the highest T_{max} (maximum weight loss temperature) at 416.2 ℃ followed by HPNFBC-*g*-PCLs. Based on the DTG curves, the thermal

decomposition of the HPNFBC-*g*-PCLs was divided into two stages, ascribed to the decomposition of HP-NFBC and PCL, respectively. The degradation temperature of HPNFBC-*g*-PCLs did not have the tendency to exhibit same degradation temperature as HP-NFBC at 277 ℃ because the content of grafted PCL is higher than HP-NFBC in both HPNFBC-g-PCL-20 (86 mol%) and HPNFBC-g-PCL-15 (78 mol%) as per confirmed by CP/MAS ^{13}C-NMR. The thermal stabilities of the HPNFBC-*g*-PCLs increased with increasing proportions of PCL. This was evidenced by the increasing T_{onset} (temperature at which sample start losing weight) (°C) and T_{max} (°C) values. HPNFBC-*g*-PCL-20, which had the highest PCL content and longest molecular chain length, displayed the highest T_{onset} and T_{max} at 334.9 and 406.8 °C, respectively (**Table 2**). For instance, the thermal stability of HPNFBC-*g*-PCL-20 was significantly improved compared to HP-NFBC, with a 20.9 % increase in the T_{onset} (**Table 2**). The enhancement in the thermal stability of HPNFBC-*g*-PCL clearly indicates that the PCL molecules were successfully introduced on the surface of the HP-NFBC fibers. It is postulated that the PCL molecules surrounding HP-NFBC fibers are responsible for the higher T_{max} might continue to increase as the molecular chain length of grafted PCL increases.

Table 2. Characterization of thermal properties of HPNFBC-*g*-PCLs, PCL, and HP-NFBC.

Sample	T_{onset}^{a} **(°C)**	T_{max}^{b} **(°C)**	T_m **(°C)**	ΔH_m **(J/g)**	T_c **(°C)**	χ_c **(%)**
HP-NFBC	277.0	372.7	-	-	-	-
HPNFBC-*g*-PCL-10	317.0	394.5	52.6	13.4	30.3	18.0
HPNFBC-*g*-PCL-15	327.4	408.9	52.9	30.9	31.9	29.0

HPNFBC-*g*-PCL-20	334.9	406.8	53.6	32.1	30.8	27.0
PCL	363.7	416.2	56.6	33.3	11.5	24.0

[a]Temperature at which sample start losing weight.; [b]Maximum weight loss temperature

Figures S11 (a) and **(b)** show the 2nd heating and 1st cooling runs of PCL and the HPNFBC-*g*-PCLs. The 2nd heating curves for the HPNFBC-*g*-PCLs and PCL showed a single endothermic peak attributed to the melting temperature (T_m), which is close to the typical melting point of PCL (58 °C) [37]. HPNFBC-*g*-PCL displayed a slightly lower T_m than that of neat PCL (M_n: 87400 g mol^{-1}), which may be attributed to the different crystal structures of the grafted and un-grafted PCL; the latter is free and has high mobility. The higher crystallization temperature displayed by all the HPNFBC-*g*-PCLs signifies that the grafting of PCL on HP-NFBC restricts the motion of PCL chain heads and aligns the chain direction, which can drastically change the crystallization behavior of PCL. HPNFBC-*g*-PCL-20 and -15 exhibited higher crystallinity than PCL despite lower T_m values, and their melting and crystalizing peaks were sharper than those of PCL, indicating their higher crystal uniformity. The PCL chains in HPNFBC-*g*-PCL-10 were of insufficient length and hence, unable to cause crystallization. Therefore, this material showed the lowest melting enthalpy and crystallinity. The crystallization temperatures of the HPNFBC-*g*-PCLs were higher than that of PCL, which could also be due to the grafting of PCL on HP-NFBC, which restricted the motion of the PCL chain heads and caused their alignment. Because PCL has a higher mobility, it requires a lower temperature for crystal growth [38,39]. Using DSC, the interaction between HPNFBC-*g*-PCL and the PCL matrix in the HPNFBC-*g*-PCL/PCL nanocomposites was also investigated (**Table S2)**. Similar to the grafted PCL, the crystallization temperature of the composites was higher than that of neat PCL, which is indicative of the enhanced intermolecular interactions between HPNFBC-*g*-PCL and the PCL matrix. The higher

enthalpy of fusion and crystallinity exhibited by the composites suggests that the presence of PCL grafted HPNFBC has further improved the nucleation growth of the matrix. However, the enthalpy of fusion and crystallinity of HPNFBC-*g*-PCL-15/PCL are inconsistent and slightly lower than those of HPNFBC-*g*-PCL-20/PCL, which may be because of some agglomeration that occurred in the PCL grafted HP-NFBC, thereby affecting its mechanical properties.

3.4. Mechanical properties of HPNFBC-g-PCL/PCL nanocomposites.

Figure 4 shows the stress-strain curves of the nanocomposites containing HPNFBC-*g*-PCL-20 and -15. The quantitative data are presented in **Table 3**. The widespread use of PCL is hindered by its extremely low Young's modulus (stiffness), as it is known to exhibit ductile behavior [40,41]. Mixing the neat PCL with PCL-grafted HP-NFBC to make 1 wt.% cellulose resulted in a conspicuous decrease in the elongation at break by 66 and 87 % in the HPNFBC-*g*-PCL-20/PCL and HPNFBC-*g*-PCL-15/PCL nanocomposites, respectively, compared to neat PCL. Moreover, the Young's modulus of neat PCL (193.6 ± 21.7 MPa) increased significantly to 661.3 ± 39.7 and 496.9 ± 32.2 MPa (**Figure 4 and Table 3**) in the HPNFBC-*g*-PCL-20/PCL and HPNFBC-*g*-PCL-15/PCL nanocomposites, respectively. Nanocomposites composed of un-grafted HP-NFBC and PCL were also prepared as the control to investigate phase compatibility (**Table S3)**. All of these nanocomposites (HP-NFBC/PCLs) showed poor mechanical properties because of the incompatibility between the filler and matrix, which was a result of the strong hydrophilic and hydrophobic natures of HP-NFBC and PCL, respectively. Further, the dumbbell shape of HP-NFBC/PCL with 13 wt.% cellulose could not be prepared because there was excessive agglomeration (**Figure S12**). However, grafting of PCL in HP-NFBC remarkably enhanced the interfacial adhesion between the PCL matrix and HP-NFBC. The mechanical behavior was thus markedly improved and the compatibility of HP-NFBC as a nanofiller was established. The

Young's modulus and ultimate strength (maximum stress) continued to increase with the addition of PCL-grafted HP-NFBC, indicating that the mechanical behavior of each nanocomposite was highly dependent on the cellulose content of the film. The HPNFBC-*g*-PCL-20/PCL nanocomposites containing 13 wt.% cellulose appeared to be the stiffest and had the most superior mechanical properties with the highest Young's modulus and highest reduction in ductility. The efficient dispersion of HPNFBC-*g*-PCL-20 in PCL contributed to the improved compatibility and interfacial adhesion, resulting in improved stress transfer upon application of a load. Therefore, the prepared materials had appreciable stiffness.

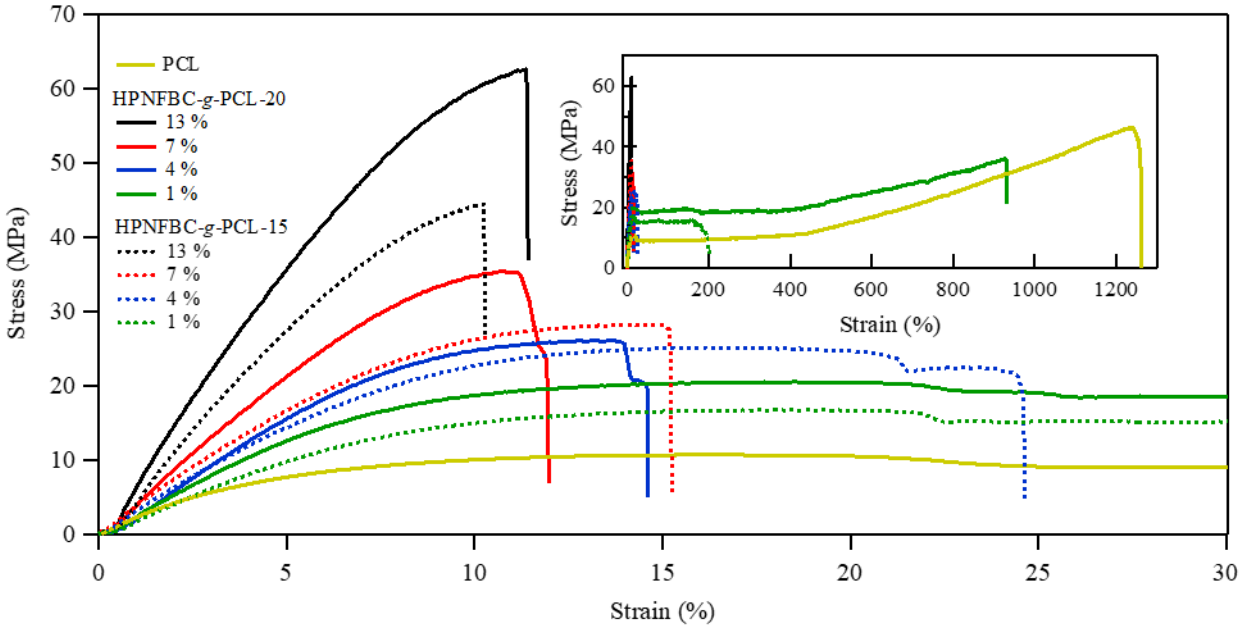

Figure 4. Stress-Strain curves of HPNFBC-*g*-PCL-20/PCL, HPNFBC-*g*-PCL-15/PCL nanocomposites with 13, 7, 4, and 1 wt.% cellulose and neat PCL.

Table 3. Mechanical properties of HPNFBC-*g*-PCL-20/PCL and HPNFBC-*g*-PCL-15/PCL nanocomposites with 13, 7, 4, and 1 wt.% cellulose and neat PCL.

Sample	**Cellulose content (wt. %)**	**Compositions[a]**		**Ultimate strength[b,c] (MPa)**	**Elongation at break[b,d] (%)**	**Young's Modulus[b,e] (MPa)**
		HPNFBC-*g*-PCL (wt. %)	**PCL (wt. %)**			
PCL (M_n, 87400; $Đ$, 1.68)	0	0	100	46.6 ± 2.3	1252 ±101.7	193.6 ± 21.7
HPNFBC-*g*-PCL-20/PCL	1	7	93	22.3 ± 2.8	426.0±204.2	224.4 ± 2.2
	4	21	79	24.8 ± 2.4	19.12 ± 5.5	286.7 ± 26.7
	7	36	64	35.6 ± 1.2	15.03 ± 2.5	397.5 ± 6.7
	13	71	29	57.3 ± 4.4	11.21 ± 1.5	661.3 ± 39.7
HPNFBC-*g*-PCL-15/PCL	1	5	95	17.5 ± 0.6	168.8 ± 23.1	186.8 ± 5.0
	4	14	86	24.2 ± 0.8	29.4 ± 6.7	248.7 ± 9.1
	7	23	77	27.5 ± 0.6	13.9 ± 1.3	299.3 ± 7.6
	13	45	55	42.7 ± 1.8	11.1 ± 0.8	496.9 ± 32.2

[a]The compositions of HPNFBC-*g*-PCL and PCL based on the calculation using Equation S5.; [b]Mean ± standard deviation.; [c]maximum stress.; [d]percentage increase in length before breaking.; [e]slope of the linear part of the elastic region.

The mechanical properties of the nanocomposites containing HPNFBC-*g*-PCL-20 and -15 were compared to study the effect of the graft length on the mechanical properties. Higher values of the ultimate strength and Young's modulus were obtained with the increase in the molecular weight of the grafted PCL. The same trend was observed for all the cellulose percentages. Longer PCL chains facilitated the interaction between HP-NFBC and the PCL matrix, which enhanced the interfacial adhesion and improved the stress transfer. Lönnberg *et al.* reported the synthesis of PCL-grafted microfibrillated cellulose using short, medium, and long PCL chains [33]. They reported that the use of long PCL-grafted one ($M_{n,SEC}$ = 26800, $Đ$ = 1.5) at a 10 wt.% cellulose content led to the most superior mechanical properties with a Young's modulus of 330 MPa, ultimate tensile strength of 27 MPa, and elongation of 18 % at break [24]. On the other hand, in our case, higher values of Young's modulus (661.3 ± 39.7 MPa), ultimate strength (57.3 ± 4.4 MPa), and elongation at break (11.21 ± 1.5 %) were obtained with a comparable cellulose content of 13 wt.%. These mechanical properties are superior to those reported thus far.

3.5. Thermomechanical properties of HPNFBC-g-PCL/PCL nanocomposites.

The thermomechanical properties were determined using TMA to determine the coefficient of thermal expansion (CTE) of the nanocomposites. The CTE is an important parameter for investigating the mechanical performance at increasing temperatures [42]. The TMA curves are shown in **Figures 5 (a)** and **(b)**. Initially, all the nanocomposites displayed a moderate change in the CTE at temperatures below the melting point of PCL. However, when the temperature exceeded the PCL melting point, a significant difference in the CTE was observed for each nanocomposite depending on the proportion of cellulose. The decrease in the CTE with increasing cellulose content was representative of the increase in the thermal dimensional stability of the PCL added to HP-NFBC. A slight enhancement was observed in the thermal dimensional stability upon

addition of 1 wt.% HP-NFBC to HPNFBC-*g*-PCL-20/PCL compared to neat PCL, whereas the CTE of HPNFBC-*g*-PCL-20/PCL nanocomposites containing 13 wt.% cellulose exhibited a 99 % decrease from 3310.3 to 32.3 ppm K^{-1}.

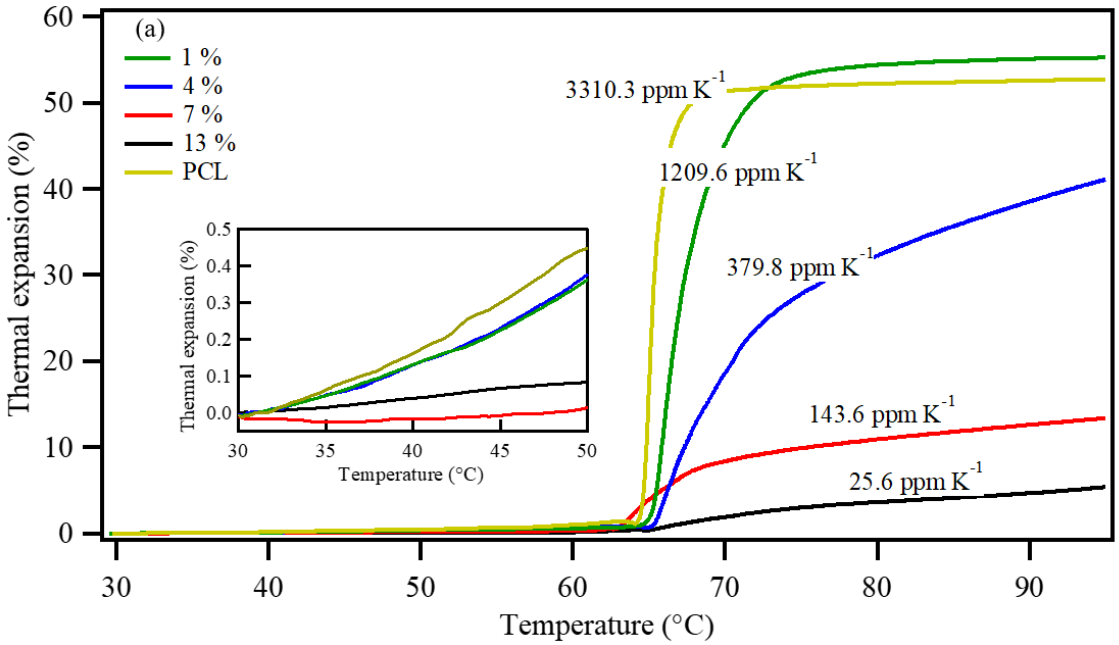

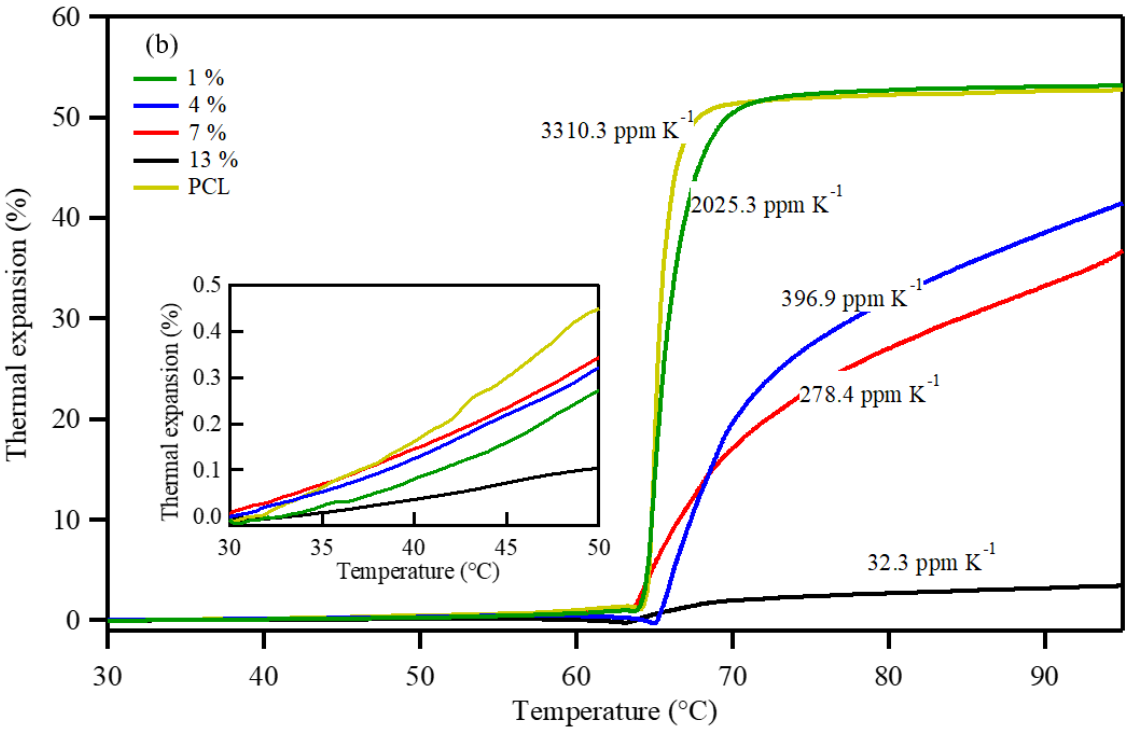

Figure 5. TMA curves of **(a)** HPNFBC-*g*-PCL-20/PCL nanocomposites **(b)** HPNFBC-*g*-PCL-15/PCL nanocomposites with 13, 7, 4, and 1 wt.% cellulose and neat PCL.

The improved thermal dimensional stability at high cellulose contents is attributed to the enhanced interfacial adhesion between the HPNFBC-*g*-PCL and neat PCL matrix, in which the high aspect ratio of HP-NFBC restricted the PCL chain relaxation, thus delaying the deformation of the PCL matrix by changing the thermal distribution inside the nanocomposites. HPNFBC-*g*-PCL-20/PCL containing 13 wt.% cellulose showed lower thermal dimensional stability than HPNFBC-*g*-PCL-20/PCL with 7 wt.% cellulose below the PCL melting point but maintained its thermal dimensional stability above the PCL melting point, whereas the CTE of HPNFBC-*g*-PCL-20 with 7 wt.% cellulose increased, which further established the superior compatibility of HP-NFBC as a nanofiller. In addition, the shorter chain length of the HPNFBC-*g*-PCL-15/PCL nanocomposites led to a lower thermal dimensional stability compared to the longer chain length of the HP-NFBC-

20/PCL nanocomposites with 1, 4, 7, and 13 wt.% cellulose contents. The addition of 1 wt.% cellulose to the HPNFBC-*g*-PCL-15/PCL nanocomposites triggered a slight drop in the CTE compared to neat PCL because of the shorter grafted PCL chain length. Moreover, the nanofiller content was insufficient to cause thermal expansion resistance in the nanocomposites. The longer chain length of the grafted PCL significantly restricted the mobility in the PCL homopolymer matrix, resulting in a lower CTE. Consistent with its highest stiffness, HPNFBC-*g*-PCL-20 containing 13 wt.% cellulose appeared to be the most stable in terms of thermal dimensional stability with the lowest CTE. The incorporation of HP-NFBC and a longer chain length can substantially improve the thermal dimensional stability of PCL.

4. Conclusions

HP-NFBC produced via a bottom-up process using *Gluconacetobacter intermedius* (NEDO-01) was successfully grafted with different chain lengths of PCL by ROP of *ε*-CL monomer initiated from the hydroxyl groups on the surface of HP-NFBC. High grafting densities of the grafted polymer chain were achieved using the efficient "grafting-from" method. PCL-grafted HP-NFBC exhibited relatively high thermal stability at 14, 22, and 45 % cellulose contents. Longer grafted PCL chain lengths led to higher crystallization temperatures and degrees of crystallinity compared to homopolymer PCL. Nanocomposites based on the PCL matrix reinforced with PCL grafted HP-NFBC were prepared by simple solvent mixing at 1, 4, 7, and 13 wt.% cellulose contents. The incorporation of only 1 wt.% cellulose significantly improved the mechanical properties, as evidenced by the enhancement in the elongation at break and Young's modulus. Remarkably, the ductile PCL became highly stiff by the incorporation of PCL grafted HP-NFBC and the ultimate stiffness was achieved at 13 wt.% of cellulose. Therefore, HP-NFBC with a very long fiber length was proved to be an excellent nanofiller for fiber-reinforced materials because of its exceptional

thermal and mechanical properties. The interfacial adhesion between HP-NFBC and the polymer matrix was significantly improved by PCL-grafting, which led to superior mechanical properties than those of most PCL-grafted cellulose nanocomposites reported previously. Based on the results of this study, the proposed strategy for grafting HP-NFBC can be extended to other systems to create high-mechanical-strength materials as an excellent alternative to unsustainable petrochemical-based materials.

Acknowledgements

We thank Mr. Yuki Kugo, Dr. Satoshi Nomura, Mr. Naoya Nakagawa, and Prof. Tomoki Erata of Hokkaido University for their support with the NMR measurements. The authors thank Prof. Ken-ichiro Matsumoto of Hokkaido University and Dr. Shuichiro Seno of Hokkaido Research Organization for their assistance with tensile testing and TMA measurements, respectively. This work was partially supported by the Hokkaido University Research and Education Center for Robust Agriculture, Forestry, and Fisheries Industry and JST-Mirai Program, Japan (Grant ID: 21461165).

Author Contributions

T.I., R.B., T.S., and **K.T.:** Conceptualization, Methodology, Writing - Review & Editing **H.H.** and **K.T.:** Data curation, Writing – Original Draft. **T.M.:** Resources. **H.H**. and **A.A.E.:** Investigation. **H.H., A.A.E., S.K.,** and **H.N.:** Formal analysis. **T.I., T.Y., R.B., T.S. and K.T.:** Supervision **K.T.:** Project administration. All authors have approved the final version of the manuscript.

References

[1] O'sullvian AC. Cellulose: the structure slowly unravels. Cellulose 1997;4:173–207.

[2] Huber GW, Iborra S, Corma A. Synthesis of transportation fuels from biomass: Chemistry, catalysts, and engineering. Chem Rev 2006;106:4044–98. https://doi.org/10.1021/cr068360d.

[3] Kose R, Sunagawa N, Yoshida M, Tajima K. One-step production of nanofibrillated bacterial cellulose (NFBC) from waste glycerol using Gluconacetobacter intermedius NEDO-01. Cellulose 2013;20:2971–9. https://doi.org/10.1007/s10570-013-0050-0.

[4] Sunagawa N, Tajima K, Hosoda M, Kawano S, Kose R, Satoh Y, et al. Cellulose production by Enterobacter sp. CJF-002 and identification of genes for cellulose biosynthesis. Cellulose 2012;19:1989–2001. https://doi.org/10.1007/s10570-012-9777-2.

[5] Kono H, Uno T, Tsujisaki H, Anai H, Kishimoto R, Matsushima T, et al. Nanofibrillated Bacterial Cellulose Surface Modified with Methyltrimethoxysilane for Fiber-Reinforced Composites. ACS Appl Nano Mater 2020;3:8232–41. https://doi.org/10.1021/acsanm.0c01670.

[6] Tajima K, Kusumoto R, Kose R, Kono H, Matsushima T, Isono T, et al. One-Step Production of Amphiphilic Nanofibrillated Cellulose Using a Cellulose-Producing Bacterium. Biomacromolecules 2017;18:3432–8. https://doi.org/10.1021/acs.biomac.7b01100.

[7] Labet M, Thielemans W. Synthesis of polycaprolactone: A review. Chem Soc Rev 2009;38:3484–504. https://doi.org/10.1039/b820162p.

[8] Woodruff MA, Hutmacher DW. The return of a forgotten polymer - Polycaprolactone in the 21st century. Prog Polym Sci 2010;35:1217–56. https://doi.org/10.1016/j.progpolymsci.2010.04.002.

[9] Bartnikowski M, Dargaville TR, Ivanovski S, Hutmacher DW. Degradation mechanisms of polycaprolactone in the context of chemistry, geometry and environment. Prog Polym Sci 2019;96:1–20. https://doi.org/10.1016/j.progpolymsci.2019.05.004.

[10] Njuguna J, Pielichowski K, Desai S. Nanofiller-reinforced polymer nanocomposites. Polym Adv Technol 2008:229–36. https://doi.org/10.1002/pat.1074.

[11] Zhang Y, Song P, Liu H, Li Q, Fu S. Morphology, healing and mechanical performance of nanofibrillated cellulose reinforced poly(ε-caprolactone)/epoxy composites. Compos Sci Technol 2016;125:62–70. https://doi.org/10.1016/j.compscitech.2016.01.008.

[12] Nakagaito AN, Yano H. The effect of fiber content on the mechanical and thermal expansion properties of biocomposites based on microfibrillated cellulose. Cellulose 2008;15:555–9. https://doi.org/10.1007/s10570-008-9212-x.

[13] Kiziltas A, Nazari B, Kiziltas EE, Gardner DJS, Han Y, Rushing TS. Cellulose NANOFIBER-polyethylene nanocomposites modified by polyvinyl alcohol. J Appl Polym Sci 2016;133:1–8. https://doi.org/10.1002/app.42933.

[14] Li K, Mcgrady D, Zhao X, Ker D, Tekinalp H, He X, et al. Surface-modified and oven-dried microfibrillated cellulose reinforced biocomposites: Cellulose network enabled high performance. Carbohydr Polym 2021;256:117525. https://doi.org/10.1016/j.carbpol.2020.117525.

[15] Li Y, Chen C, Xu J, Zhang Z, Yuan B, Huang X. Improved mechanical properties of carbon nanotubes-coated flax fiber reinforced composites. J Mater Sci 2015;50:1117–28. https://doi.org/10.1007/s10853-014-8668-3.

[16] Vega‐hernández MÁ, Cano‐díaz GS, Vivaldo‐lima E, Rosas‐aburto A, Hernández‐luna MG, Martinez A, et al. A review on the synthesis, characterization and modeling of polymer grafting. Processes 2021;9:1–85. https://doi.org/10.3390/pr9020375.

[17] Soeta H, Lo Re G, Masuda A, Fujisawa S, Saito T, Berglund LA, et al. Tailoring Nanocellulose-Cellulose Triacetate Interfaces by Varying the Surface Grafting Density of Poly(ethylene glycol). ACS Omega 2018;3:11883–9. https://doi.org/10.1021/acsomega.8b01616.

[18] Xie L, Xu F, Qiu F, Lu H, Yang Y. Single-walled carbon nanotubes functionalized with high bonding density of polymer layers and enhanced mechanical properties of composites. Macromolecules 2007;40:3296–305. https://doi.org/10.1021/ma062103t.

[19] Chadwick RC, Khan U, Coleman JN, Adronov A. Polymer grafting to single-walled carbon nanotubes: Effect of chain length on solubility, graft density and mechanical properties of macroscopic structures. Small 2013;9:552–60. https://doi.org/10.1002/smll.201201683.

[20] Stannett V. Some challenges in grafting to cellulose and cellulose derivatives 1981:3–20.

[21] Carlmark A, Larsson E, Malmström E. Grafting of cellulose by ring-opening polymerisation - A review. Eur Polym J 2012;48:1646–59. https://doi.org/10.1016/j.eurpolymj.2012.06.013.

[22] Zhou L, He H, Li MC, Huang S, Mei C, Wu Q. Grafting polycaprolactone diol onto

cellulose nanocrystals via click chemistry: Enhancing thermal stability and hydrophobic property. Carbohydr Polym 2018;189:331–41. https://doi.org/10.1016/j.carbpol.2018.02.039.

[23] Bellani CF, Pollet E, Hebraud A, Pereira F V., Schlatter G, Avérous L, et al. Morphological, thermal, and mechanical properties of poly(ε-caprolactone)/poly(ε-caprolactone)-grafted-cellulose nanocrystals mats produced by electrospinning. J Appl Polym Sci 2016;133:4–11. https://doi.org/10.1002/app.43445.

[24] Lönnberg H, Larsson K, Lindström T, Hult A, Malmström E. Synthesis of polycaprolactone-grafted microfibrillated cellulose for use in novel bionanocomposites-influence of the graft length on the mechanical properties. ACS Appl Mater Interfaces 2011;3:1426–33. https://doi.org/10.1021/am2001828.

[25] Makiguchi K, Satoh T, Kakuchi T. Diphenyl phosphate as an efficient cationic organocatalyst for controlled/living ring-opening polymerization of δ-valerolactone and ε-caprolactone. Macromolecules 2011;44:1999–2005. https://doi.org/10.1021/ma200043x.

[26] Saito T, Aizawa Y, Tajima K, Isono T, Satoh T. Organophosphate-catalyzed bulk ring-opening polymerization as an environmentally benign route leading to block copolyesters, end-functionalized polyesters, and polyester-based polyurethane. Polym Chem 2015;6:4374–84. https://doi.org/10.1039/c5py00533g.

[27] Katsuhara S, Takagi Y, Sunagawa N, Igarashi K, Yamamoto T, Tajima K, et al. Enhanced Self-Assembly and Mechanical Properties of Cellulose-Based Triblock Copolymers: Comparisons with Amylose-Based Triblock Copolymers. ACS Sustain Chem Eng 2021;9:9779–88. https://doi.org/10.1021/acssuschemeng.1c02180.

[28] Nomura S, Kugo Y, Erata T. 13C NMR and XRD studies on the enhancement of cellulose II crystallinity with low concentration NaOH post-treatments. Cellulose 2020;27:3553–63. https://doi.org/10.1007/s10570-020-03036-6.

[29] Boujemaoui A, Cobo Sanchez C, Engström J, Bruce C, Fogelström L, Carlmark A, et al. Polycaprolactone Nanocomposites Reinforced with Cellulose Nanocrystals Surface-Modified via Covalent Grafting or Physisorption: A Comparative Study. ACS Appl Mater Interfaces 2017;9:35305–18. https://doi.org/10.1021/acsami.7b09009.

[30] Roy BLF, Heinrich LA, Tayo LL, Malmström E, Engström J. Grafting of poly(ε ‐ caprolactone) from Abaca cellulose fibers via ring ‐ opening polymerization resulting in facile one ‐ pot biocomposites . SPE Polym 2021;2:297–310. https://doi.org/10.1002/pls2.10058.

[31] Olsén P, Herrera N, Berglund LA. Polymer Grafting Inside Wood Cellulose Fibers by Improved Hydroxyl Accessibility from Fiber Swelling. Biomacromolecules 2020;21:597–603. https://doi.org/10.1021/acs.biomac.9b01333.

[32] Save M, Soum A. Controlled ring-opening polymerization of lactones and lactide initiated by lanthanum isopropoxide, 2a: Mechanistic studies. Macromol Chem Phys 2002;203:2591–603. https://doi.org/10.1002/macp.200290043.

[33] Lönnberg H, Fogelström L, Berglund L, Malmström E, Hult A. Surface grafting of microfibrillated cellulose with poly(ε-caprolactone) - Synthesis and characterization. Eur Polym J 2008;44:2991–7. https://doi.org/10.1016/j.eurpolymj.2008.06.023.

[34] Hospodarova V, Singovszka E, Stevulova N. Characterization of Cellulosic Fibers by FTIR

Spectroscopy for Their Further Implementation to Building Materials. Am J Anal Chem 2018;09:303–10. https://doi.org/10.4236/ajac.2018.96023.

[35] Thongsomboon W, Serra DO, Possling A, Hadjineophytou C, Hengge R, Cegelski L. Modified Cellulose 2018;338:334–8.

[36] Ansari F, Berglund LA. Toward Semistructural Cellulose Nanocomposites: The Need for Scalable Processing and Interface Tailoring. Biomacromolecules 2018;19:2341–50. https://doi.org/10.1021/acs.biomac.8b00142.

[37] Li K, Song J, Xu M, Kuga S, Zhang L, Cai J. Extraordinary reinforcement effect of three-dimensionally nanoporous cellulose gels in poly(ε-caprolactone) bionanocomposites. ACS Appl Mater Interfaces 2014;6:7204–13. https://doi.org/10.1021/am500337p.

[38] Sakai F, Nishikawa K, Inoue Y, Yazawa K. Nucleation enhancement effect in poly(L-lactide) (PLLA)/poly(ε- caprolactone) (PCL) blend induced by locally activated chain mobility resulting from limited miscibility. Macromolecules 2009;42:8335–42. https://doi.org/10.1021/ma901547a.

[39] Zhang C, Zhai T, Turng LS, Dan Y. Morphological, Mechanical, and Crystallization Behavior of Polylactide/Polycaprolactone Blends Compatibilized by l - Lactide/Caprolactone Copolymer. Ind Eng Chem Res 2015;54:9505–11. https://doi.org/10.1021/acs.iecr.5b02134.

[40] Katsumata K, Saito T, Yu F, Nakamura N, Inoue Y. The toughening effect of a small amount of poly(ε-caprolactone) on the mechanical properties of the poly(3-hydroxybutyrate-co-3-hydroxyhexanoate)/PCL blend. Polym J 2011;43:484–92.

https://doi.org/10.1038/pj.2011.12.

[41] Hu M, Deng C, Gu X, Fu Q, Zhang J. Manipulating the Strength-Toughness Balance of Poly(l-lactide) (PLLA) via Introducing Ductile Poly(ϵ-caprolactone) (PCL) and Strong Shear Flow. Ind Eng Chem Res 2020;59:1000–9. https://doi.org/10.1021/acs.iecr.9b05380.

[42] Saba N, Jawaid M. A review on thermomechanical properties of polymers and fibers reinforced polymer composites. J Ind Eng Chem 2018;67:1–11. https://doi.org/10.1016/j.jiec.2018.06.018.